Characterization of a redox-active cross-linked complex between cyanobacterial photosystem I and its physiological acceptor flavodoxin

Mühlenhoff, Ulrich; Kruip, Jochen; Bryant, Donald A.; Rögner, Matthias; Sétif, Pierre; Boekema, Egbert

Published in:
EMBO Journal

Publication date:
1996

The EMBO Journal vol.15 no.3 pp.488–497, 1996

Characterization of a redox-active cross-linked complex between cyanobacterial photosystem I and its physiological acceptor flavodoxin

Ulrich Mühlenhoff[1], Jochen Kruip[2], Donald A.Bryant[3], Matthias Rögner[2], Pierre Sétif[4] and Egbert Boekema[5]

Institut für Biologie II, Universität Freiburg, Schänzlestraβe 1, D-79104 Freiburg, [2]Institut für Botanik, Universität Münster, Schlossgarten 3, D-48149 Münster, Germany, [3]Department of Biochemistry and Molecular Biology, Pennsylvania State University, University Park, PA 16802-4500, USA, [4]CEA, Département de Biologie Cellulaire et Moléculaire, CE Saclay, 91191 Gif-sur-Yvette Cedex, France and [5]Biofysische Chemie, Rijksuniversiteit Groningen, Nijenborgh 4, 9747 AG Groningen, The Netherlands

[1]Corresponding author

A covalent complex between photosystem I and flavodoxin from the cyanobacterium *Synechococcus* sp. PCC 7002 was generated by chemical cross-linking. Laser flash-absorption spectroscopy indicates that the bound flavodoxin of this complex is stabilized in the semiquinone state and is photoreduced to the quinol form upon light excitation. The kinetics of this photoreduction process, which takes place in ~50% of the reaction centres, displays three exponential components with half-lives of 9 μs, 70 μs and 1 ms. The fully reduced flavodoxin subsequently recombines with $P700^+$ with a $t_{1/2}$ of 330 ms. A corresponding flavodoxin semiquinone radical signal is readily observed in the dark by room temperature electron paramagnetic resonance, which reversibly disappears upon illumination. In contrast, the light-induced reduction of oxidized flavodoxin can be observed only by first-flash experiments following excessive dark adaptation. In addition, the docking site of flavodoxin on photosystem I was determined by electron microscopy in combination with image analysis. Flavodoxin binds to the cytoplasmic side of photosystem I at a distance of 7 nm from the centre of the trimer and in close contact to a ridge formed by the subunits PsaC, PsaD and PsaE.

Keywords: cyanobacteria/electron microscopy/flavodoxin/photosystem I/spectroscopy

Introduction

The net results of the light-induced electron transfer reactions in phototrophic organisms carrying a type I photosynthetic reaction centre are (i) the oxidation of periplasmic donor proteins, usually cytochromes and (ii) the reduction of a cytoplasmic pool of low-potential electron carrier proteins. These cytoplasmic proteins, usually [2Fe–2S] ferredoxins, subsequently serve as electron donors in a large variety of physiologically important processes, such as $NADP^+$ reduction, carbon fixation, nitrite/nitrate assimilation and sulfite uptake (Cammack *et al.*, 1981; Knaff and Hirasawa, 1991; Matsubara and Saeki, 1992). Besides ferredoxins, cyanobacteria may contain a low-potential flavoprotein, flavodoxin, capable of substituting ferredoxin in at least several of these ferredoxin-driven redox reactions (Rogers, 1987; Mayhew and Tollin, 1992). Flavodoxins are usually absent in cyanobacterial cells under optimal conditions of growth, although an exception occurs in the closely related chloroplasts of several rhodophytes (Fitzgerald *et al.*, 1978; Price *et al.*, 1991). However, they are inducible by iron deprivation (Hutber *et al.*, 1977; Tandeau de Marsac and Houmard, 1993).

Flavodoxins are widely distributed throughout the bacterial kingdom, serving as versatile, ubiquitous electron carrier proteins. They are usually classified according to their size as short- (16–18 kDa) or long-chain (18–20 kDa) types (Rogers, 1987; Mayhew and Tollin, 1992), with the cyanobacterial proteins belonging exclusively to the latter (Laudenbach *et al.*, 1988; Fillat *et al.*, 1991; Leonhardt and Straus, 1992). Both types are closely related, displaying the same 3-D structure with a characteristic β–α–β fold and a pocket for the non-covalently bound FMN cofactor close to the surface of the protein (Smith *et al.*, 1977, 1983; Watt *et al.*, 1991; Fukuyama *et al.*, 1992). Flavodoxins are capable of performing two successive single-electron transfer reactions, thus shuttling the redox-active FMN group between an oxidized form, a thermodynamically stabilized protonated semiquinone and a fully reduced quinol form (Mayhew and Ludwig, 1975). As substitutes for ferredoxin, flavodoxins are likely to shuttle between the semiquinone and the fully reduced form under physiological conditions (Rogers, 1987).

Because of their easily followed spectroscopic properties, flavodoxins have emerged as model systems for biological redox reactions, although most of these studies do not focus on their physiological roles (for an overview see Palma *et al.*, 1994). While the interaction with ferredoxin–$NADP^+$ oxidoreductase (FNR) has been investigated thoroughly (Pueyo and Gòmez-Moreno, 1991; Medina *et al.*, 1992a), comparatively little is known about the photoreduction of flavodoxin by photosystem I (PSI). In contrast, for ferredoxin, some features of its interaction with PSI have been proposed (see Lelong *et al.*, 1994, and references therein), and its binding site in the reaction centre has been modelled (Fromme *et al.*, 1994). Although numerous flavodoxins have been shown indirectly to replace ferredoxin as a mediator between PSI and FNR (Hutber *et al.*, 1981; Rogers, 1987; Fillat *et al.*, 1988), only one spectroscopic analysis of the photoreduction of oxidized flavodoxin by PSI (Medina *et al.*, 1992b) has so far dealt directly with the kinetic properties of this process. In addition, a protein of the photosynthetic membrane of unknown identity, presumably functioning as a flavodoxin docking protein, has been described (Pueyo and Gòmez-Moreno, 1993).

This work characterizes a chemically cross-linked complex between PSI and flavodoxin. We report the first direct observation of a physiological electron transfer reaction, preferentially employing the semiquinone–hydroquinone couple of flavodoxin, and the location of its binding site in the reaction centre by electron microscopy. Thus, flavodoxin is the first protein involved in bioenergetics for which the binding site in a membrane complex has been visualized experimentally. A detailed biochemical analysis of this covalent complex will be described in a forthcoming publication (Mühlenhoff *et al.*, 1996).

Results

Flash-absorption spectroscopy of flavodoxin reduction

The transient signals observed by laser flash-absorption spectroscopy, of a PSI preparation to which flavodoxin has been cross-linked and of a control sample pretreated with the chemical cross-linker in the absence of flavodoxin, are shown in Figure 1. The upper left chart shows the absorption changes observed at 580 nm on the control (trace 1) and the cross-linked complex (trace 2), recorded under identical experimental conditions so that the observed transients of both samples can be compared directly (see Materials and methods). This wavelength is appropriate for observing changes caused by flavodoxin because it corresponds to the absorption maximum of the protonated semiquinone form of the FMN cofactor (FH; Müller *et al.*, 1970; Entsch and Smillie, 1972; Mayhew and Ludwig, 1975). In isolated PSI, light excitation results in charge separation between $P700^+$ and the terminal acceptor, either F_A^- or F_B^-. This is monitored at 580 nm by an initial absorption decrease taking place within a few hundred nanoseconds, which can be ascribed to the formation of $(P700^+–[F_A/F_B]^-)$. Afterwards, there is practically no further absorption change during the first 5 ms following the laser flash, with the exception of some fast-decaying antenna triplet states which cannot be distinguished on this timescale ($t_{1/2}$ <15 µs; Sétif and Bottin, 1994). In contrast, in the cross-linked complex, this initial decrease is followed by a further decrease (trace 2). The difference between these two curves (trace 2 – 1) should therefore correspond to an electron transfer from PSI to flavodoxin within this complex. The large bleaching accompanying this process is indicative of the reduction of the semiquinone form of flavodoxin (FH·), because both the oxidation of $[F_A/F_B]^-$ and the reduction of oxidized flavodoxin cause an absorption increase at this wavelength. The spectral analysis described below unambiguously supports this interpretation. The decay caused by FH· reduction is multiexponential and can be fitted satisfactorily by three exponential components ($t_{1/2}$ ~9 µs, 70 µs and 1 ms; see legend to Figure 1 for details). A similar multiexponential decay is also observed in the heterologous cross-linked complex between PSI from *Synechocystis* sp. PCC 6803 and flavodoxin from *Synechococcus* sp. PCC 7002 used for electron microscopy (results not shown). An expanded part of the difference (trace 2 – 1) is shown, together with the residuals of the fit, in the upper right part of Figure 1. The fastest phase has the largest amplitude and represents >60% of the whole decay. Under the present experimental conditions, there is a dead time of 1–2 µs just after the flash, during which time the difference (trace 2 – 1) is not reliable because of the large size of the antenna triplet signals. When the fast phase is extrapolated to the time point of the flash, a small negative unresolved signal is consistently observed in such differences (trace 2 – 1). However, the amplitude of this signal is very small, and may be the result of slight distortions in the absorption properties of $[F_A/F_B]^-$ induced in the presence of covalently linked flavodoxin. To investigate further a possible modification of the properties of these terminal iron–sulfur centres in the covalent complex, the photoreduction of $[F_A/F_B]$ was studied by low-temperature electron paramagnetic resonance (EPR) spectroscopy after illumination at 15 K. The spectral characteristics of

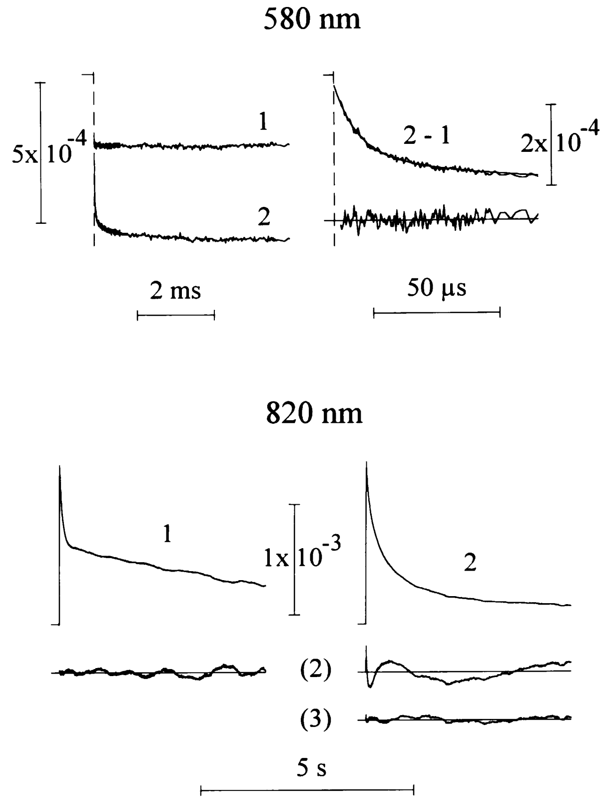

Fig. 1. Flash-induced absorption changes of PSI complexes and PSI complexes cross-linked with flavodoxin at 580 and 820 nm. Experimental conditions: 20 mM tricine, pH 8.0, 2 mM sodium ascorbate, 25 µM $DPIPH_2$ (580 nm) or 1.5 µM $DPIPH_2$ (820 nm), 0.03% β-DM, 0.23 µM PSI or PSI–flavodoxin, both from *Synechococcus* sp. PCC 7002. Band width: DC-1 MHz (580 nm) or DC-30 kHz (820 nm). Repetition rate: one flash every 10 (580 nm) or 60 s (820 nm). Average of 64 (580 nm) or 16 experiments (820 nm). Upper left: trace 1, control (treated EDC); trace 2, PSI–flavodoxin. Upper right: difference between traces 2 and 1 expanded on a 80 µs timescale. A simulated curve is also shown, together with the residuals multiplied by 3. This curve is based on the following parameters: $t_{1/2}$ = 8.9 µs (1.88×10^{-4}), 72 µs (0.88×10^{-4}) and 1.03 ms (0.41×10^{-4}), and includes an offset (3.38×10^{-4}) to take into account longer-lived absorption changes. Lower part: trace 1, control; trace 2, PSI–flavodoxin; Lower traces (2) and (3): corresponding residuals of fits with either two or three exponential components (multiplied by 3). Results of the fits: trace 1, two components, $t_{1/2}$ = 47 ms (0.75×10^{-3}) and 4.7 s (0.75×10^{-3}); trace 2, two components, $t_{1/2}$ = 167 ms (0.98×10^{-3}) and 2.6 s (0.51×10^{-3}); trace 3, three components, $t_{1/2}$ = 46 ms (0.37×10^{-3}), 325 ms (0.77×10^{-3}) and 4.4 s (0.34×10^{-3}).

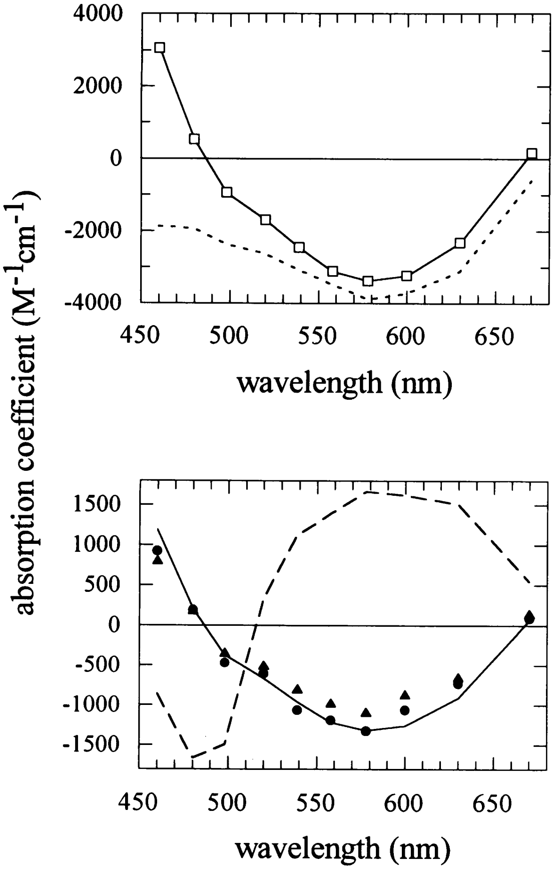

Fig. 2. Simulated and observed OD spectra of PSI-mediated redox transitions of flavodoxin. Upper part: (- - -) spectrum of the difference (flavodoxin H$^-$ – flavodoxin H·); (—□—) differential absorption spectrum corresponding to reduction of the semiquinone by $[F_A/F_B]^-$, with an absorption decrease being shown as a negative amplitude. Lower part: amplitudes observed at 50 (▲) or 800 µs (●) on signals corresponding to differences between the kinetic traces recorded in the cross-linked and control samples. Absorption coefficients were calculated by reference to the signal observed for P700$^+$ at 820 nm; (—) same spectrum as in the upper part but multiplied by a scaling factor of 0.39; (– –) differential absorption spectrum corresponding to the reduction of the oxidized flavodoxin by $[F_A/F_B]^-$. Scaling factor, 0.39.

F_A^- and F_B^- of the covalent complex were found to be identical to those observed for untreated PSI (results not shown).

Traces similar to those recorded at 580 nm were obtained from 460 to 670 nm for the control and cross-linked samples, and the corresponding differences (2 – 1) were calculated as described above. Kinetic components similar to those observed at 580 nm were found at all wavelengths. The lower part of Figure 2 shows the amplitudes observed at 50 (▲) or 800 µs (●) for the differences (2 – 1). An absorption decrease, such as that observed at 580 nm, is displayed as a negative signal. To compare these signals with the spectra expected for the reduction of either oxidized or semireduced flavodoxin by $[F_A/F_B]^-$, the differential spectra corresponding to these two single-electron reduction steps of flavodoxin were measured and combined with the differential spectrum corresponding to the single-electron reduction of $[F_A/F_B]$ (Sétif and Bottin, 1995; see Materials and methods). Figure 2 shows the calculated spectrum of the absorption changes corresponding to the reduction of the semiquinone form of flavodoxin by $[F_A/F_B]^-$ (—□—) and the spectrum corresponding to the reduction of flavodoxin semiquinone (FH$^-$–FH·) (- - -). To be directly comparable with the experimentally obtained difference spectrum, these calculated spectra for flavodoxin reduction by $[F_A/F_B]^-$ were subsequently multiplied by a scaling factor of 0.39. This factor was chosen so that all spectra corresponded to identical values when integrated between 460 and 670 nm. These are displayed in the lower graph in Figure 2. Despite some slight differences between 540 and 630 nm, the shape of the calculated spectrum for the reduction of the semiquinone by $[F_A/F_B]^-$ (—) is similar to that obtained by flash-absorption spectroscopy. However, the spectrum corresponding to the reduction of oxidized flavodoxin by $[F_A/F_B]^-$ (– –) is completely different. These spectral comparisons unambiguously show that under the employed experimental conditions the observable photoreduction process in the covalent complex corresponds to the reduction of the semiquinone form of flavodoxin to the fully reduced quinol.

In isolated PSI, charge separation is followed by charge recombination between P700$^+$ and $[F_A/F_B]^-$ (for a review see Ke, 1973). This simple mechanism should result in the monoexponential decay of P700$^+$. In contrast, a biphasic decay is generally observed for P700$^+$ in any preparation of PSI (P.Sétif, unpublished observations), such as that shown in the lower part of Figure 1 (trace 1). Such a biphasic decay can be ascribed to the competition between the expected recombination process (rate k_r) between P700$^+$ and $[F_A/F_B]^-$ and electron escape (rate k_e) from $[F_A/F_B]^-$ to exogenous acceptors, possibly oxygen and an additional acceptor of unknown origin (Rousseau *et al.*, 1993). Thus, the fast decay observed in trace 1 corresponds to both recombination and escape (rate = $k_r + k_e$), whereas the slow decay corresponds to the subsequent slow reduction of P700$^+$ by the exogenous electron donor DPIPH$_2$ (k_d) in those reaction centres where electron escape has occurred. The results of fitting trace 1 with two exponential components are given in Figure 1 [residuals (2), left] and correspond to the following values: $k_r + k_e$ ~7.3 s^{-1} and k_d ~0.15 s^{-1}.

The decay of P700$^+$ in the cross-linked sample is shown in trace 2 of the lower part of Figure 1. For this complex, the P700$^+$ reduction process appears to be different because a fit based on two exponential components does not give satisfactory results. It appears that three exponential components are necessary for a good fit [Figure 1, residuals (2) and (3), right; see the legend to Figure 1]. The fastest and slowest rates resulting from this tri-exponential fit are very similar to those found in the control PSI. About half of the total decay can be assigned to these two phases, whereas the third phase accounts for the other half (52%; rate ~2.1 s^{-1}; $t_{1/2}$ ~330 ms). These observations suggest that half of the reaction centres in the cross-linked sample undergo the same reactions as the control, while the remainder undergo a different process. We ascribe this process, which corresponds to the additional third phase present only in the cross-linked sample, to a recombination reaction between P700$^+$ and fully reduced flavodoxin (FH$^-$):

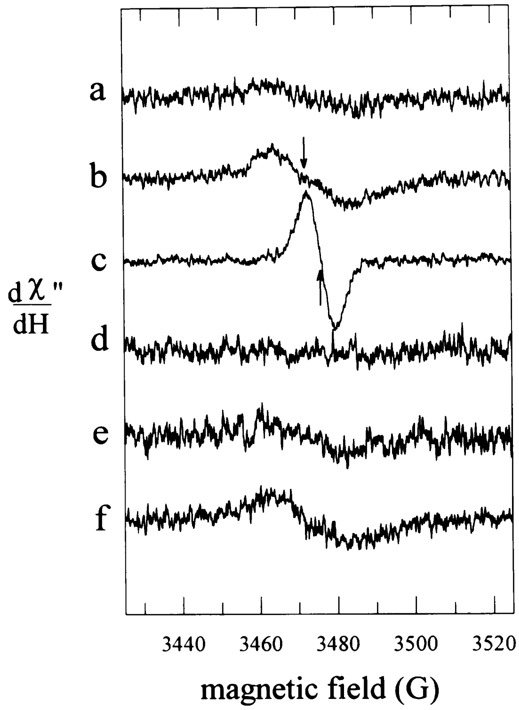

Fig. 3. EPR studies of PSI–flavodoxin cross-linked complexes. The amplitudes of the different spectra were normalized so as to be directly comparable. The EPR spectra were recorded sequentially on a single PSI–flavodoxin sample (concentration 455 μM chlorophyll, 5 mM sodium ascorbate, 50 μM $DPIPH_2$). Trace a, spectrum of the complex after storage for 1 h in the dark; trace b, spectrum accumulated in darkness just after 10 s of illumination with continuous light; trace c, spectrum accumulated under illumination; trace d, spectrum recorded in the dark just after 15 min of illumination; trace e, spectrum after 2 h in darkness in contact with air; trace f, spectrum accumulated in the dark after 1 min of illumination. The upwards and downwards arrows correspond to *g* values of 2.0026 and 2.0045, respectively.

$$P700^+\text{–}[F_A/F_B]FH^- \xrightarrow{k_{rf}} P700\text{–}[F_A/F_B]FH\cdot,$$

with k_{rf} ~2.1 s^{-1}.

EPR characterization of the covalent complex

Figure 3 shows EPR spectra recorded on a single sample of the cross-linked complex at room temperature. The first spectrum (trace a) was recorded after prolonged dark adaptation of the sample in the presence of ascorbate and $DPIPH_2$. A small signal with a peak–peak line width ΔH of ~20 G and a *g* value of ~2.0045 is observed. The same signal, but with a larger amplitude, is observed in darkness just after a short period of illumination (trace b). The above EPR characteristics of these spectra are similar to those observed previously for flavodoxin semiquinone (Crespi *et al.*, 1973; Fillat *et al.*, 1988). No signal decay was seen within 15 min after illumination. Under illumination, the preceding signal vanishes and is replaced by the spectrum of the $P700^+$ radical (trace c; ΔH ~7 G; *g* value 2.0026). After illumination for 15 min, both radicals vanish (trace d). This observation is consistent with $P700^+$ being reduced by $DPIPH_2$ and the FMN moiety being doubly reduced to FH^- during continuous illumination. Very little signal was observed later, as long as the sample stayed in the tightly closed EPR cell (results not shown). However, the FH· radical reappears when the sample is stored aerobically in darkness (trace e). This signal again increases in darkness following a short illumination (trace f). The signal size in trace f is ~80% of that in trace b. Most of these observations are consistent with the flash-absorption experiments. The flavodoxin semiquinone is very stable in darkness in the cross-linked complex and is reduced to the quinol form when illuminated (trace c). However, the quinol appears to be rather stable in the dark because no radical was detectable in trace d and at later times. This is in contrast to flash-absorption experiments, for which a flash repetition rate of 0.1 Hz can be used without any signal loss. These slightly different behaviours are probably caused by different experimental conditions. During the EPR measurements, the EPR cell was tightly closed and the samples were illuminated excessively with continuous light, while flash-absorption experiments were made aerobically using square open cuvettes. Hence, it seems reasonable that the exogenous acceptors responsible for the reoxidation of the quinol form, which most likely include dissolved oxygen, were consumed during the prolonged illumination in the EPR measurements. This state is reversed through contact with air.

Kinetic behaviour following dark adaptation

The apparent signal increase of the flavodoxin semiquinone radical in the early stage of the EPR experiments suggests that the semiquinone in the cross-linked complex can be oxidized during prolonged dark incubation (Figure 3, compare trace a with trace b). Figure 4 displays the absorption changes elicited at 580 nm in the covalent complex by a single flash after a 6 h dark incubation in an open cuvette on timescales of 60 and 1 ms. A PSI control preparation was also studied, serving as a reference (traces 0). The first- and second-flash experiments are shown in traces 1 and 2 of Figure 4, together with a trace (trace A) recorded under averaging conditions similar to those described in Figure 1. It is immediately apparent that, in contrast to traces 2 and A, an absorption increase is observed after the first flash (trace 1). This absorption increase can be ascribed to the reduction of oxidized flavodoxin by $[F_A/F_B]^-$, thus forming the semiquinone. Assuming a monoexponential process, its rate is ~145 s^{-1} ($t_{1/2}$ ~4.8 ms), which is 1.5–2.5 times smaller than the limiting rate observed previously by Medina *et al.* (1992b) for the reduction of soluble flavodoxin from *Anabaena* sp. PCC 7119 by spinach PSI. When compared with the control (trace 0 in the lower part of Figure 4), a small fast decay is observed in the first-flash experiment (trace 1), which is probably caused by the remaining semiquinone. The signal recorded after the second flash is identical to that obtained under averaging conditions (traces 2 and A). The same signal was also seen after the third and fourth flashes (results not shown). This clearly shows that 100% of the photoreducible flavodoxin of the covalent complex has been reduced to semiquinone after the first-flash excitation. First-flash experiments were also recorded with samples incubated in darkness for 0.5 and 2 h. For all time points, the amplitudes of the slower absorption increase and the faster absorption decrease relative to a control experiment are displayed in the inset of Figure 4. The two curves are approximately complementary. (Note

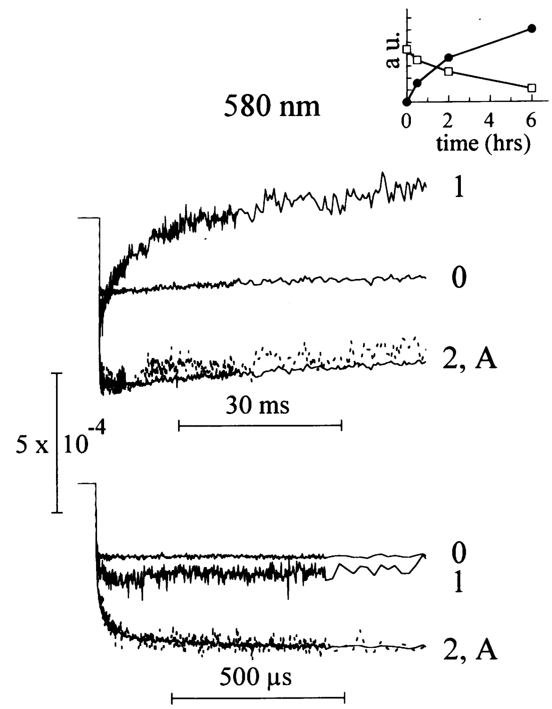

Fig. 4. Flash-induced absorption changes of dark-incubated PSI complexes. Absorption changes were recorded at 580 nm with either PSI alone (traces 0) or PSI–flavodoxin and displayed on two different timescales: upper part, 63 ms; lower part, 1 ms; traces 1 (first flash) and 2 (second flash; - - -). Single-flash experiments were recorded on a PSI–flavodoxin sample after 6 h of dark incubation. Trace A, averaged signal of 32 experiments recorded with the same complex. Inset: amplitudes of the slow absorption increase (●) and the fast absorption decrease (□) observed in the PSI–flavodoxin sample relative to the control versus the time of dark incubation. Both samples contained 0.23 μM PSI in 20 mM tricine, pH 8.0, 0.03% β-DM, 2 mM sodium ascorbate and 30 μM $DPIPH_2$.

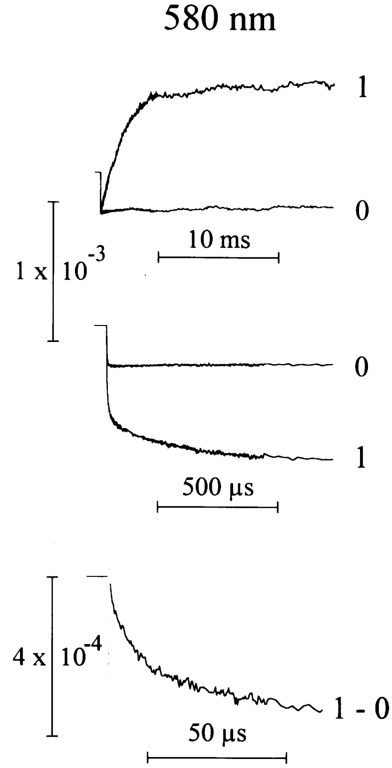

Fig. 5. Flash-induced absorption changes of the photoreduction of the oxidized (upper part) and the semiquinone forms of flavodoxin (middle and lower part) by PSI in solution measured at 580 nm. Both PSI and flavodoxin were obtained from *Synechococcus* sp. PCC 7002. Experimental conditions: 0.26 μM PSI in 50 mM tricine, pH 8.0, 0.03% β-DM, 2 mM sodium ascorbate, 15 μM DPIP, 5 mM $MgCl_2$ and 30 mM NaCl. Traces 0 are control experiments in the absence of flavodoxin; traces 1 are observed in the presence of 20.5 μM flavodoxin. For the reduction of oxidized flavodoxin (upper part), single-flash experiments were recorded after the addition of flavodoxin in complete darkness. Trace 1 corresponds to an average of four different experiments. For recording the reduction of the semiquinone form (middle part), the semiquinone was accumulated by continuous illumination of the samples for 40 s. A series of single-flash experiments was recorded just after the illumination period. The first four flashes exhibited similar kinetics and were subsequently averaged. The lower part shows the difference between a trace recorded in the presence of flavodoxin and a trace recorded in its absence after expansion on a faster timescale. The time of the flash is indicated by a vertical dotted line.

that they should not be perfectly complementary because of the contribution of $[F_A/F_B]^-$ at 580 nm.) They are both consistent with a half-life of ~2 h for semiquinone reoxidation.

Comparison with the reduction of free flavodoxin by PSI

To compare the kinetic characteristics of flavodoxin reduction in the covalent complex with that of free flavodoxin by PSI, some essential features of the latter process are shown in Figure 5, which displays the flash-induced absorption changes of this process at 580 nm. Traces 0 were recorded in the absence of flavodoxin, while traces 1 were recorded in the presence of ~20 μM flavodoxin from *Synechococcus* sp. PCC 7002. Trace 1 in the upper part of Figure 5 corresponds to first-flash experiments recorded after the addition of flavodoxin in darkness. As is the case for the covalent complex, the absorption increase can be ascribed to the formation of flavodoxin semiquinone. The signal increase can be fitted satisfactorily with a single exponential component with a rate of ~528 s^{-1}. This rate corresponds to the maximal observable rate for the photoreduction of oxidized flavodoxin, because it is close to the asymptotic value of the observed rate in a rate versus flavodoxin concentration plot (Mühlenhoff and Sétif, 1996). Again, under the employed experimental conditions the semiquinone is found to be rather stable, although to a lesser extent than in the covalent complex. This property can be employed to almost quantitatively accumulate the flavodoxin semiquinone by continuous illumination of the sample, even with flavodoxin concentrations as high as 20 μM. After such a pre-illumination, the photoreduction of flavodoxin semiquinone by PSI can be recorded, as shown in the middle part of Figure 5. The corresponding decay is biphasic, with $t_{1/2}$ values of 10 and 180 μs. A detailed study of this process will be published elsewhere, from which it is concluded that the fastest phase corresponds to a first-order process ascribed to electron transfer within a flavodoxin–PSI complex preformed before flash excitation. The observable half-life of the electron transfer process within this electrostatic complex is similar to that observed for the photoreduction of flavodoxin semiquinone in the covalent complex. The

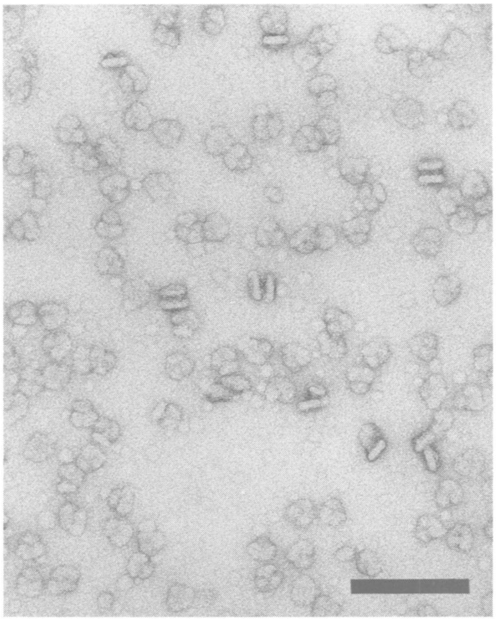

Fig. 6. Electron microscopy of trimeric PSI from *Synechocystis* sp. PCC 6803 cross-linked to flavodoxin. Part of an electron micrograph showing PSI–flavodoxin particles in top and side views. Particles were negatively stained with uranyl acetate. Scale bar represents 1000 Å.

second component corresponds to a second-order process, which is dependent upon the flavodoxin concentration (Mühlenhoff and Sétif, 1996).

Is the covalent complex capable of reducing soluble ferredoxin or flavodoxin?

The ability of the covalent complex to reduce soluble ferredoxin was investigated by comparing the kinetics of ferredoxin reduction by both this complex and PSI, pretreated with the chemical cross-linking reagents. Flash-absorption spectroscopy experiments at 580 nm (Sétif and Bottin, 1994) showed that the kinetics of ferredoxin reduction do not appear to be affected by the chemical treatment, while no ferredoxin reduction could be detected for the covalent complex at ferredoxin concentrations of up to 5 μM (results not shown). Complementarily, the ability of the cross-linked complex to reduce soluble flavodoxin was investigated using a continuous illumination assay (Xu *et al.*, 1994). In accordance with the above results, the flavodoxin photoreduction activity of a PSI preparation pretreated with the cross-linker was comparable with those of untreated PSI, while the cross-linked complex was found to be fully incapable of reducing any soluble flavodoxin (results not shown).

Analysis of projections obtained by electron microscopy

Electron micrographs, such as that shown in Figure 6, show the two characteristic views (the top and side projections) of trimeric PSI particles. By single-particle analysis, the signal:noise ratio of these projections can be enhanced greatly (Boekema *et al.*, 1994). From 16 micrographs of *Synechocystis* sp. PCC 6803 PSI particles cross-linked to flavodoxin from *Synechococcus* sp. PCC 7002, 1434 top and 29 side projections were selected for image processing. For PSI control particles treated with the chemical cross-linker in the absence of flavodoxin, 1464 top and 55 side projections were selected. The projections of the two data sets were processed separately. In each case, top projections were aligned, treated with a multivariate statistical analysis and classified to see the characteristic views with an enhanced resolution (results not shown). For final summing, only those projection classes were chosen which displayed a well-preserved 3-fold axis of rotation and sharp detail. The substantial deviation from this 3-fold symmetry of the remaining classes is mainly caused by tilting of the complexes on the carbon support of the electron micrograph. The 328 class members of these classes were pooled, and the best 125 were summed with the correlation coefficient as quality criteria (Figure 7a). Similar results were obtained from the data set of the control PSI, where 150 projections were finally summed (Figure 7b).

The height of the PSI particles was analysed from projections showing two particles aggregated in the side position with their corresponding cytoplasmic sides in close contact. The projections were aligned repeatedly on improved references and, finally, a sum was made of the best-aligned images (Figure 7c). Although the number of side views was low, the averaged side views give an indication of the overall height. The distance between the pairs of the covalent complex is estimated to be ~50 Å, and 30–35 Å for the control (results not shown). This widening out of the gap is most probably caused by flavodoxin molecules extending the overall height of the cytoplasmic side of PSI.

When the images of the cytoplasmic top views of the covalent complex and the control PSI were compared by subtraction, only one distinct difference area was seen (Figure 7d), which is interpreted as the position of flavodoxin. This flavodoxin binding site is located between the ridge formed by subunits PsaC, PsaD and PsaE and the edge of the trimer on the cytoplasmic side of the reaction centre (Figure 8). The part of the protein closest to the ridge is ~70 Å away from the 3-fold rotation axis at the centre of the trimer.

Discussion

The spectroscopic investigations of the cross-linked complex between PSI and flavodoxin clearly show that the covalent complex obtained is 'functional' in the photoreduction of the bound acceptor protein by an intramolecular electron transfer process. Therefore, it can be concluded with confidence that flavodoxin has been cross-linked correctly to its physiological binding site on the reaction centre. Both the optical and the EPR spectroscopy data clearly indicate that the observed electron transfer represents the reduction of a bound flavodoxin semiquinone to its quinol form, as long as no special experimental precautions are taken. These photoreduction events take place in ~40% of the reaction centres when monitoring the flavodoxin reduction directly by flash-absorption spectroscopy, and in ~50% of the reaction centres on the basis of the observable amplitudes assigned to a recombination between $P700^+$ and the quinol. On the other hand, the cross-linked samples are incapable of intermolecular electron transfer to any other soluble acceptor protein, indicating that the corresponding physiological binding

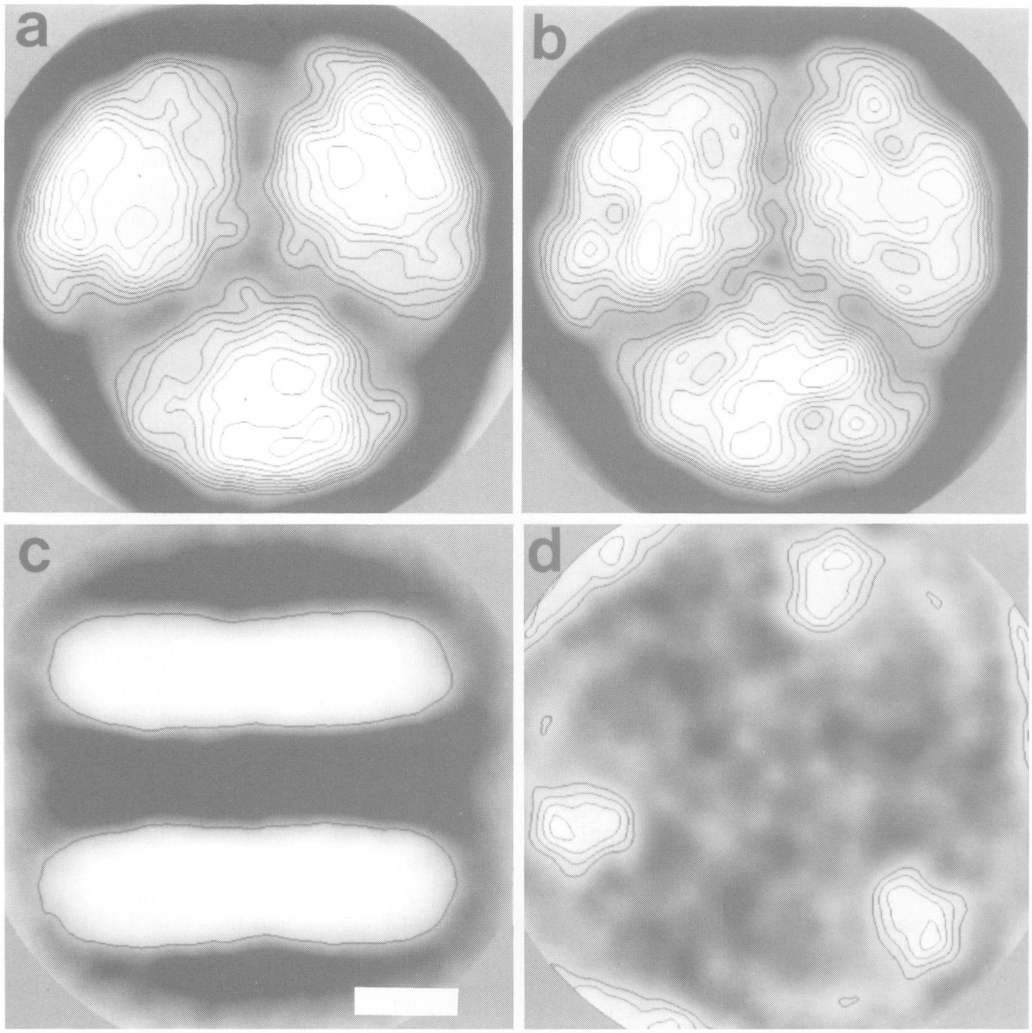

Fig. 7. Image analysis of top and side projections of trimeric *Synechocystis* sp. PCC 6803 PSI particles. (**a**) Sum of the best 125 top projections of a PSI–flavodoxin covalent complex. (**b**) Sum of the best 150 top projections of control PSI. (**c**) Sum of the 29 side projections of PSI–flavodoxin particles aggregated with their cytoplasmic sides. (**d**) Difference image between the normalized images of (a) and (b), with the lowest contour set to a level that can be expected for the outer contour of a protein with the mass of flavodoxin. Scale bar represents 50 Å.

sites in the reaction centres are completely occupied by the cross-linked acceptor protein. These observations can be reconciled by assuming that about half of the flavodoxin bound to PSI is either positioned slightly incorrectly or damaged; this may be because of a loss of the cofactor during the chemical treatment or the subsequent purification steps.

Three exponential components with half-lives of 9 μs, 70 μs and 1 ms are necessary to satisfactorily fit the absorption changes caused by reduction of the flavodoxin semiquinone. For the reduction of soluble flavodoxin semiquinone by isolated PSI, a single first-order phase with $t_{1/2}$ ~10 μs is observed, which is very similar to the fastest and major component seen in the cross-linked complex. This implies that most of the functional flavodoxin is properly attached to PSI. The two slower components observed may be a result of microheterogeneity with regard to the position of flavodoxin within the covalent complex. However, for the analogous reduction of ferredoxin by PSI, multiphasic kinetics have also been observed (Sétif and Bottin, 1994, 1995). The rate for the reduction of oxidized flavodoxin in the covalent complex is found to be approximately three times smaller than the limiting rate observed for this process in solution. This most likely reflects the fact that the protonation and structural rearrangements around the FMN cofactor accompanying this reduction step may be constrained when flavodoxin is covalently attached to PSI (Mayhew and Ludwig, 1975; Watt *et al.*, 1991). The most remarkable property of the covalent complex is the high stability of the semiquinone form of the bound flavodoxin, with a half-life for oxidation to the oxidized state in the timescale of hours. Although the semiquinone is much less reactive to oxygen than the quinol form, it is usually reoxidized within a few minutes in aqueous solutions (Mayhew and Ludwig, 1975). This process slows down in the covalent complex probably because of a decreased accessibility of the FMN site to dissolved oxygen. Very slow oxidation of the neutral semiquinone by oxygen has also been observed in several flavoenzymes (Mayhew and Ludwig, 1975), and is consistent with the observation of a flavodoxin radical *in vivo* (Crespi *et al.*, 1973).

Image analysis of negatively stained trimeric PSI particles obtained by electron microscopy visualizes details

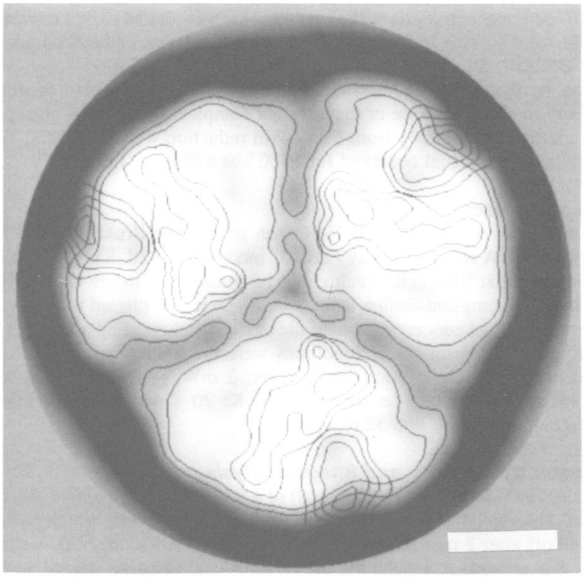

Fig. 8. Scheme for the binding of flavodoxin to PSI, as seen from the cytoplasmic side of the membrane. Indicated by contours are the areas taken by flavodoxin, and the central ridge on the cytoplasmic side of PSI, occupied by the peripheral subunits PsaC, PsaD and PsaE (determined in Kruip *et al.*, 1993 and J.Kruip, M.Rögner and E.Boekema, unpublished results) superimposed on the image shown in Figure 7b. Scale bar represents 50 Å.

with a resolution of ~2 nm, as investigated by the Fourier-ring correlation criteria (Saxton and Baumeister, 1982). At this resolution, single-particle analysis enables the localization of all PSI subunits with a mass >10 kDa by comparing projections with and without these subunits, as has been shown for subunits PsaC, PsaD and PsaE (Kruip *et al.*, 1993). The binding site of flavodoxin, obtained by a similar subtraction analysis, is located on the cytoplasmic face of the reaction centre on the outer edge of the peripheral PSI subunits. The part of the protein closest to this ridge is ~70 Å from the 3-fold rotation axis at the centre of the trimer. This position appears to be very similar to that found for ferredoxin (C.Lelong, J.Kruip, M.Rögner and E.Boekema, unpublished observations). This location of the flavodoxin docking site at the periphery of PSI is compatible with an *in vivo* trimeric organization of PSI because it provides maximal spacing between the docking sites of the individual reaction centres in the trimer. If these sites were located in a more central position, the acceptor proteins could sterically interfere with each other. In addition, this peripheral location further substantiates that the 'connecting' domain of PSI, which is located towards the centre of the trimer, is not involved in forward electron transfer.

Several structural elements on the cytoplasmic surface of PSI obtained by crystal structure analysis can be assigned to be potential structural components of the flavodoxin binding site. The view from the cytoplasmic side of PSI in Figure 8, with its central 3-fold rotation axis, corresponds completely to the top view model gained from X-ray structure analysis and can be readily superimposed (Krauss *et al.*, 1993; for a recent review, see also Golbeck, 1994). If so, the flavodoxin binding site, located on the outer left-hand side of the cytoplasmic ridge when viewed from the central rotation axis of the trimer in the electron micrograph, is positioned on the outer edge of the side of PSI carrying helix i, which has no mirror image in the current structural model. The three peripheral helices transversing this part of the reaction centre on the cytoplasmic surface are very likely elements of the flavodoxin binding site. Apparently, flavodoxin binds on their peripheral left when seen from the 3-fold rotation axis. It is probable that these helices form a part of the cytoplasmic ridge visible in the electron micrographs. The second element is the transmembrane helix M, which is in close contact to one of the three peripheral helices and which probably forms a structural part of the bottom of the site. The third element seems to be the terminal [Fe–S] centre, either F_A or F_B, which is more distant from cluster F_X because it appears to be in closer contact with flavodoxin. The distance of this cluster to the nearest edge of the flavodoxin molecule can be estimated to be <20 Å, a distance compatible with rapid electron transfer between these two partners. Thus, when compared with the two different docking sites for ferredoxin proposed after modelling the ferredoxin structure into the surface of the crystal structure of PSI (Fromme *et al.*, 1994), the flavodoxin binding site resembles only the site at which ferredoxin is positioned in the near vicinity of the terminal [Fe–S] cluster more distant to F_X.

With regard to the surfaces of flavodoxin in contact with the reaction centre, less information can be obtained from the electron micrographs alone at the given resolution. Flavodoxin is a slightly oblate protein; its dimensions are ~25×40×40 Å (Watt *et al.*, 1991). This slight asymmetricity is readily visible in the electron micrographs, suggesting that the protein is orientated in such a way that its compressed side lies almost perpendicular to the plane of the photosynthetic membrane. As estimated from the increased gap between the individual trimers in the side projections, the overall height of the cytoplasmic face of PSI increases by 15–20 Å in the presence of flavodoxin. Attributing this increase to flavodoxin implies that at least half of the molecule (20–25 Å) is buried within PSI. Furthermore, to enable electron transfer, the FMN binding pocket must be orientated towards the central part of the cytoplasmic ridge of PSI and is therefore shielded from the view onto the cytoplasmic surface in Figure 8. Hence, the surface of flavodoxin directly opposite this pocket is located on the edge of the reaction centre. In addition, the contour lines of the visible surface of the flavodoxin molecule suggest an increase in the overall height towards the edge of the reaction centre. This is compatible with the general appearance of flavodoxin, but at the available resolution the rigid structure of flavodoxin precludes an unambiguous identification of its visible surface in the electron micrographs. However, the assigned structural elements of PSI involved in flavodoxin binding will allow an unambiguous modelling of this protein into the crystallographic structure. The result of this model will provide an insight into the surface areas of flavodoxin in close contact with the reaction centre, which in turn may lead to a better understanding of the electron pathway from PSI to flavodoxin.

Materials and methods

Biological materials

Recombinant flavodoxin. The *isiB* gene of *Synechococcus* sp. PCC 7002 (Leonhardt and Straus, 1992) was modified by site-directed mutagenesis, to create an *Afl*III restriction site at the start codon, and inserted into the *Nco*I and *Eco*RI sites of pSE280 (Brosius, 1989). Flavodoxin was overproduced in *Escherichia coli* strain BL21(DE3). Cells were harvested 4 h after induction with 0.6 mM IPTG and lysed using a French press. Flavodoxin was purified by a combination of anion-exchange and gel filtration chromatography, essentially as described by Fillat *et al.* (1991). A pure protein was obtained, as judged by SDS–PAGE. The preparation was incubated at a concentration of 500 μM flavodoxin with 5 mM FMN for 3–4 days at 4°C. Excessive cofactor was subsequently removed by gel filtration. A spectral ratio A_{276}/A_{466} ~0.19 was observed routinely, comparable with those for flavodoxins purified from cyanobacterial cells (Hutber *et al.*, 1981). 20–40 mg of purified protein are routinely obtained from 1 l of cells.

PSI preparations. PSI from *Synechococcus* sp. PCC 7002 was isolated essentially as described by Golbeck *et al.* (1988), except that 0.03% (w/v) β-dodecyl-maltoside (β-DM) was used in the sucrose-gradient centrifugation step. PSI from *Synechocystis* sp. PCC 6803 was isolated as described by Rögner *et al.* (1990) and Kruip *et al.* (1993). The trimeric status of the preparations from both organisms was confirmed by HPLC gel filtration.

Chemical cross-linking. PSI at a concentration of 75 μg/ml chlorophyll was incubated in the presence and absence of 10 μM flavodoxin with 3 mM *N*-ethyl-3-[3-(dimethylamino)-propyl]-carbodiimide (EDC) in 20 mM MOPS, pH 6.5, 5 mM $MgCl_2$ and 0.03% (w/v) β-DM for 30 min at 25°C in the dark. The reaction was terminated by the addition of ammonium acetate, pH 7.8, to a final concentration of 0.1 M and concentrated 4-fold by diafiltration. The reaction centre was recovered by sucrose-gradient centrifugation. Samples prepared for electron microscopy were purified by gel filtration on an HPLC column, as described by Rögner *et al.* (1990).

Evaluation of the OD spectra of the redox transitions of flavodoxin

The spectra of flavodoxin from *Synechococcus* sp. PCC 7002 were recorded from 350 to 700 nm in 1×1 cm cuvettes with flavodoxin concentrations of ~35 μM. The neutral semiquinone form of flavodoxin (FH·) was obtained at pH 5.8 by adding 10 mM sodium dithionite and 0.5 μM benzylviologen. The fully reduced form (FH^-) was obtained at pH 9.1 by adding 10 mM sodium dithionite and 0.5 μM methylviologen. Contributions of dithionite and the viologens were subtracted from the spectra. The differential absorption coefficients were calculated assuming an absorption coefficient of 9500 $M^{-1}cm^{-1}$ for oxidized flavodoxin at 466 nm (Hutber *et al.*, 1981). With this last assumption, a value of 3900 $M^{-1}cm^{-1}$ was measured for the absorption coefficient of the semiquinone at 580 nm. The differential spectra corresponding to the reduction of the oxidized form of flavodoxin to the semiquinone and the second reduction of the semiquinone to the quinol form by $[F_A/F_B]^-$ were calculated by combining the corresponding (F_{ox} – FH·) and (FH· – FH^-) difference spectra and the differential spectra corresponding to the single-electron reduction of $[F_A/F_B]^-$. The OD spectrum for the single-electron reduction of $[F_A/F_B]$ was measured by flash-absorption spectroscopy in PSI from *Synechocystis* 6803, as described previously (Sétif and Bottin, 1994).

Flash-absorption spectroscopy

Measurements were made at 296 K, with microsecond time resolution and with 6 ns full width at half maximum, as described previously (Sétif and Bottin, 1994). Square cuvettes (1×1 cm) were used. The repetition rate of laser flash excitation used for averaging was 0.1 Hz. The measuring wavelength was selected by two interference filters placed before and after the cuvette. To minimize the actinic effects of the measuring light during measurements in the visible region, a shutter was placed in front of the cuvette and opened 1 ms before flash excitation. Kinetic data were fitted to a multiexponential decay with a Marquardt least-squares algorithm.

For identifying absorption signals caused by the reduction of flavodoxin in the cross-linked complex, a control cuvette was studied containing PSI pretreated with EDC in the absence of flavodoxin. The absorption spectra of the two cuvettes (control and cross-linked samples) were adjusted at the red maximum of chlorophyll (ΔOD = 1.2–1.4 at 679 nm). The margin of error was <0.2% and the spectra of the two samples were found to be identical in the whole visible region (ΔOD <0.004). PSI concentrations of the samples were calculated from the photoinduced absorption changes at 820 nm, assuming an absorption coefficient of 6500 $M^{-1}cm^{-1}$ for $P700^+$ at this wavelength (Mathis and Sétif, 1981). The $P700^+$ concentrations of the two samples were found to be identical within <1.0%. This indicates that the antenna content of both samples was identical, thus allowing to extract reliably the absorption changes caused by flavodoxin by the subtraction of the traces observed for the control sample from those of the covalent complex. Differential absorption coefficients resulting from flavodoxin reduction were calculated by reference to the signal observed for $P700^+$ at 820 nm.

EPR spectroscopy

Measurements were made at 296 K with an X-band Bruker ESP300E spectrometer. A standard cavity (TE 102 mode) was used. Samples were studied in a flat EPR cell which could be illuminated inside the cavity by an 800 W tungsten–iodine lamp, whose beam was filtered to remove infrared light and concentrated onto the cavity window using a Plexiglas light pipe. The experimental conditions were the following: microwave frequency, 9.743 GHz; microwave power, 2 mW; modulation, 2 G at 100 kHz; gain, 8×10^4; temperature 296 K; 20 s per sweep; and an average of between 8 and 32 experiments.

Electron microscopy and image analysis

For electron microscopy, a drop (4 μl) of a PSI particle suspension (~0.5 mg/ml chlorophyll) was prepared on carbon-coated grids, which were blotted off after 2 min. The grids were washed once with distilled water for a few seconds to reduce the background, and negative stained with 2% uranyl acetate. Electron microscopy was performed with a Jeol JEM 1200 EX electron microscope with 80 kV at approximately ×60 000 magnification. Electron micrographs were digitized with a Kodak Eikonix Model 1412 CCD camera using a scan step size of 25 μm.

An image analysis was carried out on a Convex C220 computer using IMAGIC software. In the first step after the particle selection, all selected images were bandpass filtered to remove the very fine and very coarse image features (Harauz *et al.*, 1988). In the next step, the images were aligned using correlation techniques, starting with one noisy single projection as a first reference. Subsequent references were constructed from the sums of the best-aligned particles from a previous alignment (Harauz *et al.*, 1988). In the following step, the aligned non-symmetrical particles were submitted to a multivariate statistical analysis and automatic classification, as described previously (Harauz *et al.*, 1988; Boekema *et al.*, 1989). The members of each class were summed, but in a slightly different way than that described previously (Kruip *et al.*, 1993). For the final sums, the images to be summed were shifted rotationally and translationally using the parameters that were calculated when they were aligned with the bandpass filter imposed. In the last step, final sums were 3-fold rotationally symmetrized.

Acknowledgements

We wish to thank Dr W.Keegstra for his help with computer image analysis, Mr K.Gilissen for photography and Dr W.Nitschke for discussions. This work was supported by The Netherlands Foundation for Chemical Research, with financial aid from The Netherlands Organization for Scientific Research. D.A.B. acknowledges the financial support from the National Science Foundation (grant DMB-9206851). U.M. and M.R. acknowledge the financial support of the Deutsche Forschungsgemeinschaft.

References

Boekema,E.J., Dekker,J.P., Rögner,M., Witt,I., Witt,H.T. and van Heel,M.G. (1989) Refined analysis of the trimeric structure of the isolated photosystem I complex from the thermophilic cyanobacterium *Synechococcus* sp. *Biochim. Biophys. Acta*, **974**, 81–87.

Boekema,E.J., Boonstra,A.F., Dekker,J.P. and Rögner,M. (1994) Electron microscopic structural analysis of photosystem I, photosystem II and the cytochrome *b6/f* complex from green plants and cynobacteria. *J. Bioenerg. Biomembr.*, **26**, 17–29.

Brosius,J. (1989) Superpolylinkers in cloning and expression vectors. *DNA*, **8**, 759–777.

Cammack,R., Rao,K.K. and Hall,D.O. (1981) Metalloproteins in the evolution of photosynthesis. *Bio-Systems*, **14**, 57–80.

Crespi,H.L., Norris,J.R., Bays,J.P. and Katz,J.J. (1973) ESR and NMR studies with deuterated flavodoxin. *Ann. N.Y. Acad. Sci.*, **222**, 178–179.

Entsch,B. and Smillie,R.M. (1972) Oxidation–reduction properties of phytoflavin, a flavoprotein from blue-green algae. *Arch. Biochem. Biophys.*, **151**, 378–386.

Fillat,M.F., Sandmann,G. and Gòmez-Moreno,C. (1988) Flavodoxin from the nitrogen-fixing cyanobacteria *Anabaena* PCC 7119. *Arch. Microbiol.*, **150**, 160–164.

Fillat,M.F., Borrais,W.E. and Weisbeek,P.J. (1991) Isolation and overexpression in *Escherichia coli* of the flavodoxin gene from *Anabaena* PCC 7119. *Biochem. J.*, **280**, 187–191.

Fitzgerald,M.P., Husain,A. and Rogers,L.J. (1978) A constitutive flavodoxin from a eucaryotic alga. *Biochem. Biophys. Res. Commun.*, **81**, 630–635.

Fromme,P., Schubert,W.D. and Krauss,N. (1994) Structure of photosystem I: suggestions on the docking sites for plastocyanin, ferredoxin and the coordination of P700. *Biochim. Biophys. Acta*, **1187**, 99–105.

Fukuyama,K., Matsubara,H. and Rogers,L.J. (1992) Crystal structure of oxidized flavodoxin from a red alga *Chondrus crispus* at 1.6 Å resolution. *J. Mol. Biol.*, **225**, 775–789.

Golbeck,J.H. (1994) Photosystem I. In Bryant,D.A. (ed.), *The Molecular Biology of Cyanobacteria.* Kluwer Academic Publishers, Dordrecht, The Netherlands, pp. 319–360.

Golbeck,J.H., Parrett,K.G., Mehari,T., Jones,K.L. and Brand,J.J. (1988) Isolation of the intact photosysem I reaction center core containing P700 and the iron-sulfur center F_X. *FEBS Lett.*, **228**, 268–272.

Harauz,G., Boekema,E.J. and Van Heel,M. (1988) Statistical analysis of electron micrographs of ribosomal subunits. *Methods Enzymol.*, **164**, 35–49.

Hutber,G.N., Hutson,K.G. and Rogers,L.J. (1977) Effect of iron deficiency on levels of two ferredoxins and flavodoxin in a cyanobacteria. *FEMS Microbiol. Lett.*, **1**, 193–196.

Hutber,G.N., Smith,A.J. and Rogers,L.J. (1981) Flavodoxin from the blue-green alga *Nostroc* strain MAC. *Phytochemistry*, **20**, 383–387.

Ke,B. (1973) The primary electron acceptor of photosystem I. *Biochim. Biophys. Acta*, **301**, 1–33.

Knaff,D.B. and Hirasawa,M. (1991) Ferredoxin-dependent chloroplast enzymes. *Biochim. Biophys. Acta*, **1056**, 93–125.

Krauss,N. *et al.* (1993) Three-dimensional structure of system I of photosynthesis at 6 Å resolution. *Nature*, **361**, 326–330.

Kruip,J., Boekema,E.J., Bald,D., Boonstra,A.F. and Rögner,M. (1993) Isolation and structural characterization of monomeric and trimeric photosystem I complexes ($P700–F_A/F_B$ and $P700–F_X$) from the cyanobacterium *Synechocystis* PCC 6803. *J. Biol. Chem.*, **268**, 23353–23360.

Laudenbach,D.E., Reith,M.E. and Straus,N.A. (1988) Isolation, sequence analysis and transcriptional studies of the flavodoxin gene from *Anacystis nidulans* R2. *J. Bacteriol.*, **170**, 258–265.

Lelong,C., Sétif,P., Lagoutte,B. and Bottin,H. (1994) Identification of the amino acids involved in the functional interaction between photosystem I and ferredoxin from *Synechocystis* sp. PCC 6083 by chemical cross-linking. *J. Biol. Chem.*, **269**, 10034–10039.

Leonhardt,K. and Straus,N.A. (1992) An iron stress operon involved in the photosynthetic electron transport in the marine cyanobacterium *Synechococcus* sp. PCC 7002. *J. Gen. Microbiol.*, **138**, 1613–1621.

Mathis,P. and Sétif,P. (1981) Near infra-red absorption spectra of the chlorophyll *a* cations and triplet states *in vitro* and *in vivo*. *Isr. J. Chem.*, **21**, 316–320.

Matsubara,H. and Saeki,K. (1992) Structural and functional diversity of ferredoxins and related proteins. In Cammarck,R. (ed.), *Advances in Inorganic Chemisty.* Academic Press, San Diego, CA, Vol. 38, pp. 223–280.

Mayhew,S.G. and Ludwig,M.L. (1975) Flavodoxins and electron-transferring flavoproteins. In Boyer,P.D. (ed.), *The Enzymes.* Academic Press, London, UK, Vol. XII, pp. 57–118.

Mayhew,S.G. and Tollin,G. (1992) General properties of flavodoxins. In Müller,F. (ed.), *Chemistry and Biochemistry of Flavoenzymes.* CRC Press, Boca Raton, FL, Vol. III, pp. 389–426.

Medina,M., Peleato,M.L., Mendez,E. and Gòmez-Moreno,C. (1992a) Identification of specific carboxyl groups on *Anabaena* PCC 7119 flavodoxin which are involved in the interaction with ferredoxin–$NADP^+$ reductase. *Eur. J. Biochem.*, **203**, 373–379.

Medina,M., Hervas,M., Navarro,J.A., De la Rosa,M.A., Gòmez-Moreno,C. and Tollin,G. (1992b) A laser-flash absorption spectroscopy study of *Anabaena* sp. PCC 7119 flavodoxin photoreduction by photosystem I particles from spinach. *FEBS Lett.*, **313**, 239–242.

Mühlenhoff,U. and Sétif,P. (1996) Laser flash absorption spectroscopy study of flavodoxin reduction by photosystem I in *Synechococcus* sp. PCC 7002. *Biochemistry*, **35**, in press.

Mühlenhoff,U., Zhao,J. and Bryant,D.A. (1996) Interaction of photosystem I and flavodoxin from the cyanobacterium *Synechococcus* sp. PCC 7002 as revealed by chemical crosslinking. *Eur. J. Biochem.* **235**, in press.

Müller,F., Hemmerich,P., Ehrenberg,A., Palmer,G. and Massey,V. (1970) The chemical and electronic structure of the neutral flavin radical as revealed by electron spin resonance spectroscopy of chemically and isotopically substituted derivatives. *Eur. J. Biochem.*, **14**, 185–196.

Palma,P.N., Moura,I., LeGall,J., Van Beeumen,J., Wampler,J.E. and Moura,J.J.G. (1994) Evidence for a ternary complex formed between flavodoxin and cytochrome c_3. ^{1}H-NMR and molecular modelling studies. *Biochemistry*, **33**, 6394–6407.

Price,N.T., Smith,A.J. and Rogers,L.J. (1991) Isolation of flavodoxin isoforms from a macroalga *Porphyra umbilicalis* and a conformational change on dissociation of flavin. *Phytochemistry*, **30**, 2835–2839.

Pueyo,J.J. and Gòmez-Moreno,C. (1991) Characterization of the cross-linked complex formed between ferredoxin–$NADP^+$ reductase and flavodoxin from *Anabaena* PCC 7119. *Biochim. Biophys. Acta*, **1059**, 149–156.

Pueyo,J.J. and Gòmez-Moreno,C. (1993) Interaction of flavodoxin with cyanobacterial thylakoids. *Photosynthesis Res.*, **38**, 35–39.

Rogers,L.J. (1987) Ferredoxins, flavodoxins and related proteins: structure, function and evolution. In Fay,P. and Van Baalen,C. (eds), *The Cyanobacteria.* Elsevier Publishers, Amsterdam, The Netherlands, pp. 35–67.

Rögner,M., Dixon,P.J. and Diner,B.A. (1990) Purification and characterization of photosystem I and photosystem II core complexes from wild-type and phycocyanin-deficient strains of the cyanobacterium *Synechocystis* sp. PCC 6803. *J. Biol. Chem.*, **265**, 6189–6196.

Rousseau,F., Sétif,P. and Lagoutte,B. (1993) Evidence for the involvement of PSI-E subunit in the reduction of ferredoxin by photosystem I. *EMBO J.*, **12**, 1755–1765.

Saxton,W.O. and Baumeister,W. (1982) Image averaging for biological specimens: the limits imposed by imperfect crystallinity. *J. Microsc.*, **127**, 127–138.

Sétif,P. and Bottin,H. (1994) Laser flash absorption spectroscopy study of ferredoxin reduction by photosystem I in *Synechocystis* sp. PCC 6803: evidence for submicrosecond and microsecond kinetics. *Biochemistry*, **33**, 8495–8504.

Sétif,P. and Bottin,H. (1995) Laser flash absorption spectroscopy study of ferredoxin reduction by photosystem I: spectral and kinetic evidence for the existence of several photosystem I–ferredoxin complexes. *Biochemistry*, **34**, 9059–9070.

Smith,W.W., Burnett,R.M., Darling,G.D. and Ludwig,M.L. (1977) Structure of the semiquinone form of flavodoxin from *Clostridium* MP. *J. Mol. Biol.*, **117**, 195–225.

Smith,W.W., Pattridge,K.A., Ludwig,M.L., Petsko,G.A., Tsernoglou,D., Tanaka,M. and Yasunobu,K.T. (1983) Structure of flavodoxin from *Anacystis nidulans*. *J. Mol. Biol.*, **165**, 737–755.

Tandeau de Marsac,N. and Houmard,J. (1993) Adaptation of cyanobacteria to environmental stimuli: new steps towards molecular mechanism. *FEMS Microbiol. Rev.*, **104**, 119–190.

Watt,W., Tulinsky,A., Swenson,R.P. and Watenpaugh,K.D. (1991) Comparison of the crystal structures of flavodoxin in its three oxidation states at cryogenic temperatures. *J. Mol. Biol.*, **218**, 195–208.

Xu,Y., Jung,Y.S., Chitnis,V.P., Guikema,J.A., Golbeck,J.H. and Chitnis,P.R. (1994) Mutational analysis of photosystem I polypeptides in *Synechocystis* sp. PCC 6803. *J. Biol. Chem.*, **269**, 21512–21518.

Received on July 14, 1995; revised on October 12, 1995